

# When No-Reference Image Quality Models Meet MAP Estimation in Diffusion Latents

Weixia Zhang, *Member, IEEE*, Dingquan Li, *Member, IEEE*, Guangtao Zhai, *Fellow, IEEE*, Xiaokang Yang, *Fellow, IEEE*, and Kede Ma, *Senior Member, IEEE*

**Abstract**—Contemporary no-reference image quality assessment (NR-IQA) models can effectively quantify perceived image quality, often achieving strong correlations with human perceptual scores on standard IQA benchmarks. Yet, limited efforts have been devoted to treating NR-IQA models as natural image priors for real-world image enhancement, and consequently comparing them from a perceptual optimization standpoint. In this work, we show—for the first time—that NR-IQA models can be plugged into the maximum a posteriori (MAP) estimation framework for image enhancement. This is achieved by performing gradient ascent in the diffusion latent space rather than in the raw pixel domain, leveraging a pretrained *differentiable* and *bijective* diffusion process. Likely, different NR-IQA models lead to different enhanced outputs, which in turn provides a new computational means of comparing them. Unlike conventional correlation-based measures, our comparison method offers complementary insights into the respective strengths and weaknesses of the competing NR-IQA models in perceptual optimization scenarios. Additionally, we aim to improve the best-performing NR-IQA model in diffusion latent MAP estimation by incorporating the advantages of other top-performing methods. The resulting model delivers noticeably better results in enhancing real-world images afflicted by unknown and complex distortions, all preserving a high degree of image fidelity.

**Index Terms**—No-reference image quality assessment, Real-world image enhancement, Perceptual optimization, Model comparison, Diffusion models.

## I. INTRODUCTION

IMAGE quality assessment (IQA) models have been widely investigated [1] as proxies of human observers to gauge perceived image quality. Depending on whether original reference images are available, IQA models fall under two broad categories: full-reference IQA (FR-IQA) [2], [3] and no-reference IQA (NR-IQA) [4], [5]. FR-IQA models are most suitable when original undistorted images are accessible. However, in many real-world scenarios, it is inherently difficult, if not impossible, to specify ideal reference outputs [6]. This highlights the critical need for NR-IQA models to assess perceived image quality in the absence of pristine references.

Beyond their utility in performance evaluation, IQA models also show great promise for guiding perceptual optimization of image processing systems. FR-IQA models have long

played this role, from the era of measuring error visibility and structural similarity [2] to more recent data-driven approaches [3], [7]. Notably, a comprehensive comparison of FR-IQA models applied to the optimization of various image processing algorithms has been carried out [8], effectively turning the perceptual optimization process into an analysis-by-synthesis framework [9]. A natural question then arises:

*Can we rely on NR-IQA models for perceptual optimization, and evaluate them by comparing their respective optimized results?*

An immediate approach to tackle this question is to directly optimize an existing NR-IQA model  $q_w(x) : \mathbb{R}^M \mapsto \mathbb{R}$ , parameterized by  $w$ , with respect to the input image  $x$ . In other words, one seeks

$$x^* = \arg \max_x q_w(x), \quad (1)$$

where a higher value of  $q_w(x)$  indicates better predicted quality, and  $x^* \in \mathbb{R}^M$  denotes the resulting optimized image. Because of the high dimensionality and non-convexity of this maximization, the fidelity of the optimized image is implicitly constrained through the specification of the initial image  $x^{\text{init}}$ . However, as discussed in [10] and illustrated in Fig. 1(b), even when  $q_w(\cdot)$  is instantiated by a state-of-the-art NR-IQA model (LIQE [11] in this case), the optimized image often comes with severe local texture and color distortions, resulting in degraded visual quality relative to the initial.

A straightforward next step is to treat  $q_w(\cdot)$  as a natural image prior, and substitute it into the standard maximum a posteriori (MAP) framework, leading to the optimization:

$$\begin{aligned} x^* &= \arg \min_x E(x|x^{\text{init}}) \\ &= \arg \min_x D_0(x, x^{\text{init}}) - \lambda q_w(x), \end{aligned} \quad (2)$$

where the posterior  $p(x|x^{\text{init}}) \propto \exp(-E(x|x^{\text{init}}))$  is written in terms of its corresponding Gibbs energy. Here,  $D_0(\cdot, \cdot) : \mathbb{R}^M \times \mathbb{R}^M \mapsto \mathbb{R}$  denotes the fidelity term (also known as the negative log-likelihood term), which can be instantiated by an FR-IQA method. The hyperparameter  $\lambda$  mediates the trade-off between the likelihood and the prior. As shown in Fig. 1(c), even with a visually optimal choice of  $\lambda$ , the MAP-enhanced image remains no better than the initial, which manifests itself as a visually imperceptible adversarial example of the NR-IQA model [10]. As  $\lambda$  increases, the resulting visual artifacts become increasingly pronounced (see Fig. 2), converging to the result of direct maximization of  $q_w(\cdot)$ .

Weixia Zhang, Guangtao Zhai, and Xiaokang Yang are with the MoE Key Lab of Artificial Intelligence, AI Institute, Shanghai Jiao Tong University, Shanghai, China (e-mail: {zwx8981, zhaiguangtao, xkyang}@sjtu.edu.cn).

Dingquan Li is with the Department of Networked Intelligence, Pengcheng Laboratory, Shenzhen, China (e-mail: dingquanli@pku.edu.cn).

Kede Ma is with the Department of Computer Science and Shenzhen Research Institute, City University of Hong Kong, Kowloon, Hong Kong (e-mail: kede.ma@cityu.edu.hk).



Fig. 1. (a) Distorted image used as the initial point. (b) Optimized image obtained by directly maximizing a state-of-the-art NR-IQA model, LIQE [11] (see Eq. (1)). (c) Optimized image generated via MAP estimation (see Eq. (2)), where the likelihood term is implemented by the mean squared error (MSE) and LIQE [11] is employed as the prior. (d) Optimized image produced by diffusion latent MAP estimation (see Eq. (17)). Below each image is its LIQE-predicted quality score, which ranges up to a maximum of five. A larger value indicates higher predicted quality.

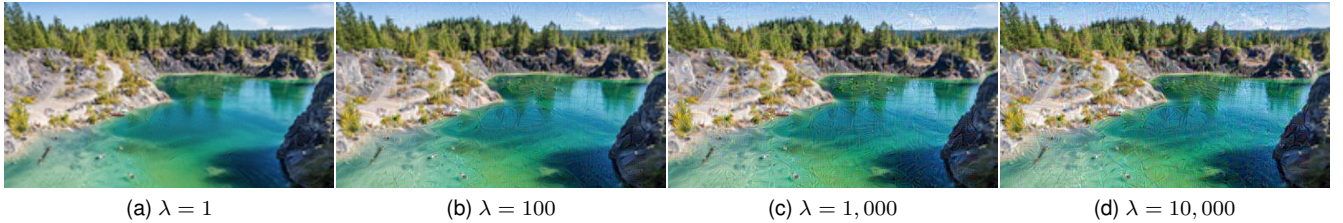


Fig. 2. Optimized images via MAP estimation (see Eq. (2)) for various values of  $\lambda$ .

In this work, for the first time, we show that contemporary NR-IQA models can be used for perceptual optimization within the MAP estimation framework (see Fig. 1(d)). Inspired by [12], we augment an NR-IQA method with a *differentiable* and *bijective* diffusion transform. This enhancement equips the NR-IQA model with generative capabilities to better represent the rich diversity of natural images by operating in the diffusion latent space<sup>1</sup>. Concretely, we work with the method of exact diffusion inversion via coupled transformations (EDICT) [13], which utilizes affine coupling [14], [15] to turn any pretrained diffusion model into a bijection between the input image and the corresponding latent noise vector.

By performing MAP estimation in the diffusion latent space, we arrive at a new computational method of comparing NR-IQA models within an analysis-by-synthesis framework. In particular, we incorporate eight NR-IQA models into this framework to “enhance” a collection of photographic images distorted by real-world visual distortions [16]–[18]. Through *debiased* psychophysical testing [6] on these optimized images, we reveal the relative performance of the competing NR-IQA models in real-world image enhancement. These findings offer complementary insights for the future NR-IQA model development beyond traditional fixed-set correlation-based evaluations.

As a preliminary effort, we improve the best-performing NR-IQA model in our psychophysical experiment, LIQE [11], by integrating the multi-scale image representation from the second-best model MUSIQ [19] and retraining it on a combined IQA dataset [16], [17], [20]–[23]. The resulting improved LIQE offers significantly better enhancement of real-

world images plagued by complex distortions, while maintaining comparable quality assessment accuracy.

In summary, our contributions are three-fold.

- We introduce the computational framework of diffusion latent MAP estimation, allowing “imperfect” NR-IQA models to serve as natural image priors for perceptual optimization of real-world image enhancement methods.
- Leveraging this framework, we perform a systematic comparison of eight contemporary NR-IQA models, yielding several noteworthy insights.
- Drawing on these insights, we improve a state-of-the-art NR-IQA model by combining aspects of multiple top-performing models, resulting in improved performance in real-world image enhancement.

## II. RELATED WORK

In this section, we begin by surveying the progress in NR-IQA. Next, we examine model comparison approaches through the lens of analysis by synthesis [9], [24]. Finally, we provide an overview of diffusion models, highlighting their applications across various computer vision tasks.

### A. NR-IQA Models

In its early stage, NR-IQA predominantly hinged on hand-crafted natural scene statistics [4], [25]–[27], followed by a regression step for quality prediction. Although these techniques proved useful within constrained scenarios, they struggled to handle the broad range of image content and distortion types found in real-world scenarios. With the emergence of deep learning, researchers shifted toward end-to-end optimization of deep neural networks (DNNs) for NR-IQA, thereby eliminating the need for hand-engineered features. Nevertheless, the efficacy of these models remains limited by the small scale of human perceptual data—often encapsulated as mean

<sup>1</sup>We distinguish between “latent diffusion”, where the diffusion process is carried out in the latent space instead of the raw pixel space, and “diffusion latent”, which treats the diffusion process as a feature transform, with the pure noise vector serving as the latent representation.

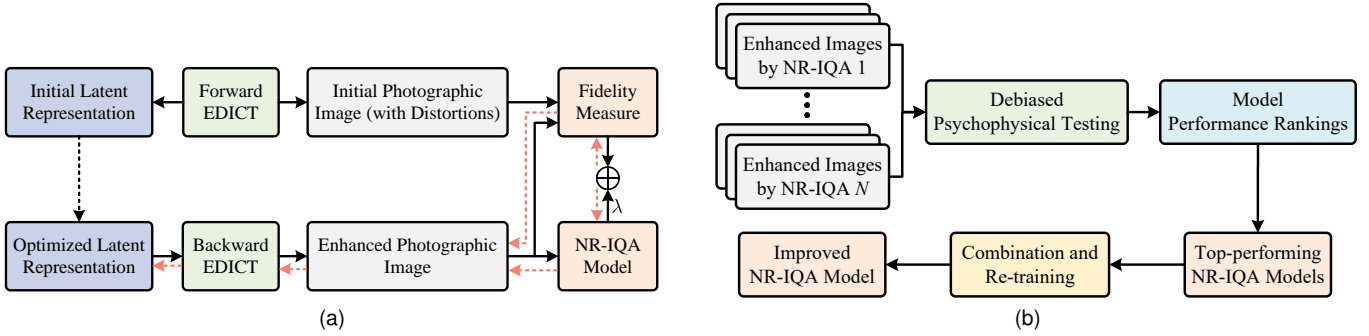


Fig. 3. (a) System diagram of diffusion latent MAP estimation. (b) NR-IQA model comparison and improvement enabled by the proposed diffusion latent MAP estimation framework.

opinion scores (MOSs). To mitigate this challenge, various data-efficient strategies have since been introduced, including patch-wise training [5], quality-aware pretraining [28]–[30], learning from pseudo-labels [31], [32], meta-learning [33], contrastive learning [34]–[37], and multitask learning [11], [18], [38]. Building on these, the NR-IQA community has more recently shifted its focus to more practical and robust solutions, such as predicting local quality variations [39], addressing subpopulation shifts [40]–[43], designing more powerful architectures [19], [44], [45], and leveraging multi-modal information [46]–[49].

### B. Model Comparison Methods

Model comparison is integral to model development [50]. Conventional model comparison entails assembling a static test set with ground-truth measurements and assessing how well different computational models align with it. Rather than seeking to validate a model purely through this discriminative approach, one can alternatively test it in a generative way, an approach encapsulated by analysis-by-synthesis in Grenander’s Pattern Theory [9], [24]. Representative generative model comparison methods include the maximum differentiation (MAD) competition [51], eigen-distortion analysis [52], and controversial stimuli synthesis [53]. While the core idea remains similar, the synthesis procedure can be reframed as discretized sample selection from a large-scale unlabeled image set, enabling broader applicability to tasks such as IQA [54], image recognition [55], semantic segmentation [56], image enhancement [6], and large language modeling [57]. Our work is closely related to the perceptual attack of NR-IQA models [10], as both can be cast into MAP estimation, yet they diverge substantially in design goals and technical details. The perceptual attack measures the adversarial robustness of NR-IQA models against visually imperceptible perturbations in the pixel space, while our method operates in the diffusion latent space, focusing on how well NR-IQA models perform in real-world image enhancement.

### C. Diffusion Models

Diffusion models form a class of generative models aimed at reversing a noise-adding procedure that unfolds over multiple steps [58]. The literature recognizes three main variants of

these models: 1) denoising diffusion probabilistic models [59], [60], which draw inspiration from non-equilibrium thermodynamics [61], 2) noise-conditioned score networks [62], trained via score matching [63] to learn the gradients of the log-likelihood of noisy data, and 3) stochastic differential equations [64], which offer a unified view that generalizes the first two approaches. Diffusion models have achieved remarkable results across a wide range of image synthesis tasks [65]–[67]. For more precise control over generated outcomes, both classifier guidance [65] and classifier-free guidance [68] have been proposed, albeit at their respective costs of training noise-aware classifiers and class-conditional diffusion models. In the context of photographic image editing [69], diffusion inversion (*i.e.*, recovering the noise vector that produces the photographic image to be edited via reverse diffusion) becomes a key requirement. EDICT [13] provides an elegant solution by converting any pretrained diffusion model into a differentiable bijection through affine coupling [14], [15]. Compared with other alternatives (*e.g.*, denoising diffusion implicit models [70]), EDICT enables exact diffusion inversion without the need for extra training or knowledge distillation. Taking inspiration from [12], we integrate NR-IQA models with EDICT to enable MAP estimation in the diffusion latent space for real-world image enhancement. Our approach stands in clear contrast to current diffusion-based image enhancers, which typically introduce additional modules to pretrained diffusion models [71]–[74], and/or adjust their sampling procedures [75]–[78]. The proposed diffusion latent MAP estimation framework not only works in tandem with those modified diffusion models through EDICT, but also offers a post-enhancement step for further improving the visual quality of their outputs (see Sec. V-D).

## III. DIFFUSION LATENT MAP ESTIMATION

In this section, we first present the necessary preliminaries of diffusion models, with a specific focus on EDICT [13]. We then introduce the proposed diffusion latent MAP estimation framework for real-world image enhancement, and employ it to compare NR-IQA models. Fig. 3 shows the system diagram.

### A. Preliminaries

For a photographic image  $x \in \mathbb{R}^M$ , potentially subject to realistic complex distortions, the objective of an NR-IQA

model  $q_w(\mathbf{x})$  is to estimate the perceived quality of  $\mathbf{x}$  such that it well aligns with the underlying MOS  $q(\mathbf{x}) \in \mathbb{R}$ .

We also work with a diffusion model [79] to transform images. In the forward diffusion process, a set of timesteps  $\{\alpha_t\}_{t=0}^T$  is defined, where  $\alpha_0 = 1$  and  $\alpha_T = 0$ , representing a monotonically increasing noise schedule. During this process, the input image  $\mathbf{x}_0$  is perturbed at the  $t$ -th step:

$$\mathbf{x}_t = \sqrt{\alpha_t}\mathbf{x}_0 + \sqrt{1 - \alpha_t}\boldsymbol{\epsilon}, \quad (3)$$

where  $\boldsymbol{\epsilon} \sim \mathcal{N}(\mathbf{0}, \mathbf{I})$ . In the reverse diffusion process, which corresponds to data generation, a denoising network  $\boldsymbol{\epsilon}_\theta(\cdot; t) : \mathbb{R}^M \mapsto \mathbb{R}^M$ , parameterized by  $\theta$  and  $t$ , is trained to progressively remove the noise [70]:

$$\begin{aligned} \hat{\mathbf{x}}_{t-1} &= \sqrt{\alpha_{t-1}} \frac{\hat{\mathbf{x}}_t - \sqrt{1 - \alpha_t} \boldsymbol{\epsilon}_\theta(\hat{\mathbf{x}}_t; t)}{\sqrt{\alpha_t}} + \sqrt{1 - \alpha_{t-1}} \boldsymbol{\epsilon}_\theta(\hat{\mathbf{x}}_t; t) \\ &= a_t \hat{\mathbf{x}}_t + b_t \boldsymbol{\epsilon}_\theta(\hat{\mathbf{x}}_t; t), \end{aligned} \quad (4)$$

where  $a_t = \sqrt{\alpha_{t-1}/\alpha_t}$ ,  $b_t = -\sqrt{\alpha_{t-1}(1 - \alpha_t)/\alpha_t} + \sqrt{1 - \alpha_{t-1}}$ , and  $\hat{\mathbf{x}}_T = \boldsymbol{\epsilon}$ . The success of the diffusion model largely relies on the denoising network  $\boldsymbol{\epsilon}_\theta(\cdot; t)$ , which is optimized by minimizing

$$\mathbb{E}_{\mathbf{x}_0, \boldsymbol{\epsilon} \sim \mathcal{N}(\mathbf{0}, \mathbf{I}), t} [\lambda(t) \|\boldsymbol{\epsilon} - \boldsymbol{\epsilon}_\theta(\mathbf{x}_t; t)\|_2^2], \quad (5)$$

where  $\lambda(t)$  is a positive weight for time step  $t$ , and  $\mathbf{x}_t$  is derived from  $\mathbf{x}_0$  according to Eq. (3). However, this denoising process is not fully invertible due to the linearization assumption  $\boldsymbol{\epsilon}_\theta(\hat{\mathbf{x}}_t; t) = \boldsymbol{\epsilon}_\theta(\hat{\mathbf{x}}_{t-1}; t)$ , which does not hold strictly.

Noticing the resemblance between the denoising process in diffusion models and the affine coupling operation in normalizing flows [14], [15], Wallace *et al.* [13] ensured invertibility in Eq. (4) by maintaining two coupled noise vectors (and their intermediate states):

$$\mathbf{x}_{t-1} = a_t \mathbf{x}_t + b_t \boldsymbol{\epsilon}_\theta(\mathbf{y}_t; t), \quad (6)$$

$$\mathbf{y}_{t-1} = a_t \mathbf{y}_t + b_t \boldsymbol{\epsilon}_\theta(\mathbf{x}_{t-1}; t), \quad t \in \{1, \dots, T\}, \quad (7)$$

where  $\mathbf{x}_T = \mathbf{y}_T = \boldsymbol{\epsilon}$ . Here we strip off the ‘‘hat’’ symbol in the math notations to highlight the bijective nature of Eqs. (6) and (7). To improve numerical stability and maintain faithfulness to the original diffusion dynamics, a mixing operation is introduced, leading to the following denoising process:

$$\mathbf{x}'_t = a_t \mathbf{x}_t + b_t \boldsymbol{\epsilon}_\theta(\mathbf{y}_t; t), \quad (8)$$

$$\mathbf{y}'_t = a_t \mathbf{y}_t + b_t \boldsymbol{\epsilon}_\theta(\mathbf{x}'_t; t), \quad (9)$$

$$\mathbf{x}_{t-1} = p \mathbf{x}'_t + (1 - p) \mathbf{y}'_t, \quad (10)$$

$$\mathbf{y}_{t-1} = p \mathbf{y}'_t + (1 - p) \mathbf{x}_{t-1}, \quad t \in \{1, \dots, T\}, \quad (11)$$

where  $p \in [0, 1]$  is a mixing parameter designed to alleviate deviations from the linearization assumption.

Eqs. (8) to (11) can be linearly inverted, yielding a deterministic noising process, which serves as a feature transform:

$$\mathbf{y}'_t = (\mathbf{y}_{t-1} - (1 - p) \mathbf{x}_{t-1})/p, \quad (12)$$

$$\mathbf{x}'_t = (\mathbf{x}_{t-1} - (1 - p) \mathbf{y}'_t)/p, \quad (13)$$

$$\mathbf{y}_t = (\mathbf{y}'_t - b_t \boldsymbol{\epsilon}_\theta(\mathbf{x}'_t; t))/a_t, \quad (14)$$

$$\mathbf{x}_t = (\mathbf{x}'_t - b_t \boldsymbol{\epsilon}_\theta(\mathbf{y}_t; t))/a_t, \quad t \in \{1, \dots, T\}. \quad (15)$$

We collectively denote the differentiable and bijective feature transform from the coupled input images  $(\mathbf{x}_0, \mathbf{y}_0)$ , where  $\mathbf{y}_0 =$

---

### Algorithm 1 Diffusion Latent MAP Estimation Solver

---

**Require:** An NR-IQA model  $q_w(\cdot)$ , an FR-IQA model as the image fidelity measure  $D_0(\cdot, \cdot)$ , an EDICT model to map a photographic image into a diffusion latent space  $\mathbf{d}(\cdot)$  and its inversion  $\mathbf{h}(\cdot)$ , # of optimization steps MaxIter, # of diffusion steps  $T$ , the trade-off parameter  $\lambda$ , the momentum parameter  $\rho$ , and the learning rate  $\alpha$

**Input:** An initial image  $\mathbf{x}^{\text{init}}$

**Output:** A pair of optimized images  $(\mathbf{x}^*, \mathbf{y}^*)$  with nearly identical content and enhanced perceptual quality

---

```

1:  $\mathbf{m}_x = \mathbf{0}, \mathbf{m}_y = \mathbf{0}$ 
2:  $(\mathbf{x}_T, \mathbf{y}_T) \leftarrow \mathbf{d}(\mathbf{x}^{\text{init}}, \mathbf{x}^{\text{init}})$ 
3: for  $i = 1 \rightarrow \text{MaxIter}$  do
4:    $(\mathbf{x}, \mathbf{y}) \leftarrow \mathbf{h}(\mathbf{x}_T, \mathbf{y}_T)$ 
5:    $\ell(\mathbf{x}_T) \leftarrow D_0(\mathbf{x}, \mathbf{x}^{\text{init}}) - \lambda q_w(\mathbf{x})$ 
6:    $\ell(\mathbf{y}_T) \leftarrow D_0(\mathbf{y}, \mathbf{x}^{\text{init}}) - \lambda q_w(\mathbf{y})$ 
7:    $\ell(\mathbf{x}_T, \mathbf{y}_T) \leftarrow (\ell(\mathbf{x}_T) + \ell(\mathbf{y}_T))/2$ 
8:    $\Delta\ell(\mathbf{x}_T) \leftarrow \partial\ell(\mathbf{x}_T, \mathbf{y}_T)/\partial\mathbf{x}_T$ 
9:    $\Delta\ell(\mathbf{y}_T) \leftarrow \partial\ell(\mathbf{x}_T, \mathbf{y}_T)/\partial\mathbf{y}_T$ 
10:   $(\mathbf{m}_x, \mathbf{m}_y) \leftarrow \rho(\mathbf{m}_x, \mathbf{m}_y) - \alpha(\Delta\ell(\mathbf{x}_T), \Delta\ell(\mathbf{y}_T))$ 
11:   $(\mathbf{x}_T, \mathbf{y}_T) \leftarrow (\mathbf{x}_T, \mathbf{y}_T) + (\mathbf{m}_x, \mathbf{m}_y)$ 
12: end for
13:  $(\mathbf{x}^*, \mathbf{y}^*) \leftarrow \mathbf{h}(\mathbf{x}_T, \mathbf{y}_T)$ 

```

---

$\mathbf{x}_0$ , to the noise representation  $(\mathbf{x}_T, \mathbf{y}_T)$  as  $\mathbf{d}(\cdot) : \mathbb{R}^{2M} \mapsto \mathbb{R}^{2M}$ . Its inverse, denoted by  $\mathbf{d}^{-1}$ , is represented as  $\mathbf{h}(\cdot) : \mathbb{R}^{2M} \mapsto \mathbb{R}^{2M}$ , correspondingly.

### B. Diffusion Latent MAP Estimation

In Bayesian statistics, the MAP estimate of an unknown quantity, as a point estimate, is the mode of its posterior distribution. In the context of image enhancement, MAP estimation can be expressed as

$$\begin{aligned} \mathbf{x}^* &= \arg \max_{\mathbf{x}} p(\mathbf{x} | \mathbf{x}^{\text{init}}) = \arg \max_{\mathbf{x}} p(\mathbf{x}^{\text{init}} | \mathbf{x}) p(\mathbf{x}) \\ &= \arg \min_{\mathbf{x}} -\log p(\mathbf{x}^{\text{init}} | \mathbf{x}) - \log p(\mathbf{x}). \end{aligned} \quad (16)$$

Here, the first term measures the fidelity of the enhanced image  $\mathbf{x}$  with respect to the initial input  $\mathbf{x}^{\text{init}}$ . This is commonly implemented by the mean squared error (MSE) to admit efficient (iterative) solvers via techniques like half-quadratic splitting [80]. Other FR-IQA models can also be employed. The second term captures the naturalness of the image. Common choices for this term include various regularization techniques and priors, such as total variation regularization [81], Gaussian scale mixture priors [82], (non-local) patch-based priors [83], sparsity regularization [84], low-rank priors [85], deep image priors [86], and adversarial loss functions [87].

As discussed in the Introduction, it is enticing to plug NR-IQA models as priors into MAP estimation to guide optimization toward the highest-quality image in the vicinity of the initial  $\mathbf{x}^{\text{init}}$ . However, conventional NR-IQA models are trained in a *discriminative* manner on finite datasets of limited distortion types, making them less effective as naturalness priors (as shown in Fig. 1). Building on the insights from [12], we address this limitation by augmenting existing NR-IQA

models with a differentiable and bijective diffusion model  $\mathbf{h}(\cdot)$ , as described in Sec. III-A. This augmentation imbues NR-IQA models with generative capabilities, enabling MAP estimation in the diffusion latent space:

$$\mathbf{x}_T^* = \arg \min_{\mathbf{x}_T} D(\mathbf{h}(\mathbf{x}_T), \mathbf{x}^{\text{init}}) - \lambda q_w(\mathbf{h}(\mathbf{x}_T)), \quad (17)$$

where we omit the coupled noise vector  $\mathbf{y}_T$  for notation simplicity. Eq. (17) can be conveniently solved using gradient-based optimization, as outlined in Algorithm 1. Empirically, the optimized image pair  $(\mathbf{x}^*, \mathbf{y}^*)$  exhibits near-identical content and appearance, aligning with the observations in [12].

### C. NR-IQA Model Comparison

By plugging various NR-IQA models into diffusion latent MAP estimation (in Eq. (17)), we can generate multiple enhanced versions of the same input image, each differing in color and detail reproduction. This motivates us to formalize NR-IQA model comparison through diffusion latent MAP estimation. Specifically, we first compile a large-scale dataset of photographic images with realistic complex distortions, denoted as  $\mathcal{X} = \{\mathbf{x}^{(i)}\}_{i=1}^{|\mathcal{X}|}$ . Next, we plug each of  $N$  NR-IQA models  $\{q_j(\cdot)\}_{j=1}^N$  into the diffusion latent MAP estimation framework, producing a total of  $|\mathcal{X}| \times N$  enhanced images,  $\{\{\mathbf{r}_j(\mathbf{x}^{(i)})\}_{i=1}^{|\mathcal{X}|}\}_{j=1}^N$ . Here,  $\mathbf{r}_j(\cdot) : \mathbb{R}^M \mapsto \mathbb{R}^M$  denotes the entire enhancement process, achieved by solving diffusion latent MAP estimation with the  $j$ -th NR-IQA model, as described in Algorithm 1. Comparing all these enhanced images through complete psychophysical testing is impractical due to its time-consuming and labor-laborious nature. Instead, we adopt an efficient and debiased psychophysical testing procedure [6]. For any pair of NR-IQA models  $q_i(\cdot)$  and  $q_j(\cdot)$ , corresponding to their respective enhancers  $\mathbf{r}_i(\cdot)$  and  $\mathbf{r}_j(\cdot)$ , we automatically select a subset of  $K$  images (where  $K \ll |\mathcal{X}|$ ) that best differentiate between the models by maximizing their enhancement discrepancy:

$$\tilde{\mathbf{x}}^{(k+1)} = \arg \max_{\mathbf{x} \in \mathcal{X}/\mathcal{S}^{(k)}} D_1(\mathbf{r}_i(\mathbf{x}), \mathbf{r}_j(\mathbf{x})) + \gamma D_2(\mathbf{x}, \mathcal{S}^{(k)}), \quad (18)$$

where  $\mathcal{S}^{(k)} = \{\tilde{\mathbf{x}}^{(k')}\}_{k'=1}^k$  represents the set of  $k$  images already selected by iteratively solving the above equation.  $D_1(\cdot, \cdot) : \mathbb{R}^M \times \mathbb{R}^M \mapsto \mathbb{R}$  represents the perceptual distance between two images.  $D_2(\cdot, \cdot) : \mathbb{R}^M \times \mathcal{P}(\mathbb{R}^M) \mapsto \mathbb{R}$ , where  $\mathcal{P}(\cdot)$  is the power set function (excluding the empty set) that computes the semantic distance between an image and an image set as a measure of content diversity. The hyperparameter  $\gamma$  trades off the two terms. The definitions of  $D_1(\cdot, \cdot)$  and  $D_2(\cdot, \cdot)$  are consistent with the original configuration described in [6]. Once  $\tilde{\mathbf{x}}^{(k+1)}$  is identified, it is added into the set  $\mathcal{S}^{(k)}$  to form  $\mathcal{S}^{(k+1)}$ .

Consequently, we generate  $KN(N-1)$  image pairs, which are then subject to formal psychophysical testing using a two-alternative forced choice (2AFC) method. During each trial, subjects are presented with a pair of enhanced images of the same content, each corresponding to a different NR-IQA model. They are allowed unlimited viewing time to select the image they perceive as higher quality. More details regarding the psychophysical experiment are given in Sec. IV-A. After

testing, the raw human perceptual data are compiled into an  $N \times N$  matrix  $\mathbf{C}$ , where  $C_{ij}$  records the empirical probability that  $q_i(\cdot)$  is chosen over  $q_j(\cdot)$ . Under the Thurstone Case V assumption [88], the global ranking scores of NR-IQA models  $\boldsymbol{\mu} = [\mu_1, \mu_2, \dots, \mu_N]^\top$  can be obtained via maximum likelihood estimation for multiple options [89]:

$$\ell_{\boldsymbol{\mu}}(\mathbf{C}) = \sum_{ij} C_{ij} \Phi\left(\frac{\mu_i - \mu_j}{\sqrt{2}\sigma}\right), \quad \text{s.t.} \sum_{i=1}^N \mu_i = 0, \quad (19)$$

where  $\Phi(\cdot)$  denotes the standard Gaussian cumulative distribution function. The parameter  $\sigma$  (*i.e.*, the standard deviation in the observer model) is fixed to 1.0484, so that one unit of the just-objectionable difference corresponds to 75% of the population selecting one image over the other [90]. A linear constraint is imposed to resolve the translation ambiguity.

## IV. EXPERIMENTS

In this section, we first describe the selection of test photographic images to be enhanced and competing NR-IQA models, followed by other implementation details. We proceed by presenting and analyzing the model comparison results.

### A. Experimental Setups

**Image Selection.** We select 500 photographic images, displaying realistic complex distortions from three IQA datasets: LIVE Challenge [16], KonIQ-10k [17], and SPAQ [18] to form  $\mathcal{X}$ . Unlike simulated image enhancement tasks with simple, clear goals (*e.g.*, image denoising and deblurring), we address the challenge of enhancing images afflicted by mixed, complex distortions [16]. Such distortions, introduced during the image acquisition process and ensuing processing steps, do not fall neatly into simple specific categories (see Fig. 4). All images are resized to  $512 \times 512$  pixels via bicubic interpolation and center cropping. We exclude images that are of extremely low-quality or lack a clear foreground subject, since enhancement in these cases offers limited potential for quality discrimination or semantic improvement.

**Model Selection.** We choose eight state-of-the-art NR-IQA models that illustrate diverse design philosophies.

- **NIQE** [25] is a knowledge-driven, training-free approach that computes quality by measuring the distance of a test image to a corpus of undistorted natural images in a quality-aware feature space.
- **DBCNN** [30] uses two specialized CNN streams—one pretrained to classify synthetic distortion types and levels, and the other leveraging a pretrained VGG-16 [91] for authentic distortions—whose features are bilinearly pooled for quality prediction.
- **HyperIQA** [92] is a self-adaptive method that learns to apply perception rules via a hyper-network for quality prediction.
- **PaQ-2-PiQ** [39] is a deep region-based method trained on FLIVE [39], leveraging both global-to-local and local-to-global feedback to yield global quality predictions as well as local quality maps.
- **UNIQUE** [40] is a unified and uncertainty-aware NR-IQA model for synthetic and realistic distortions by

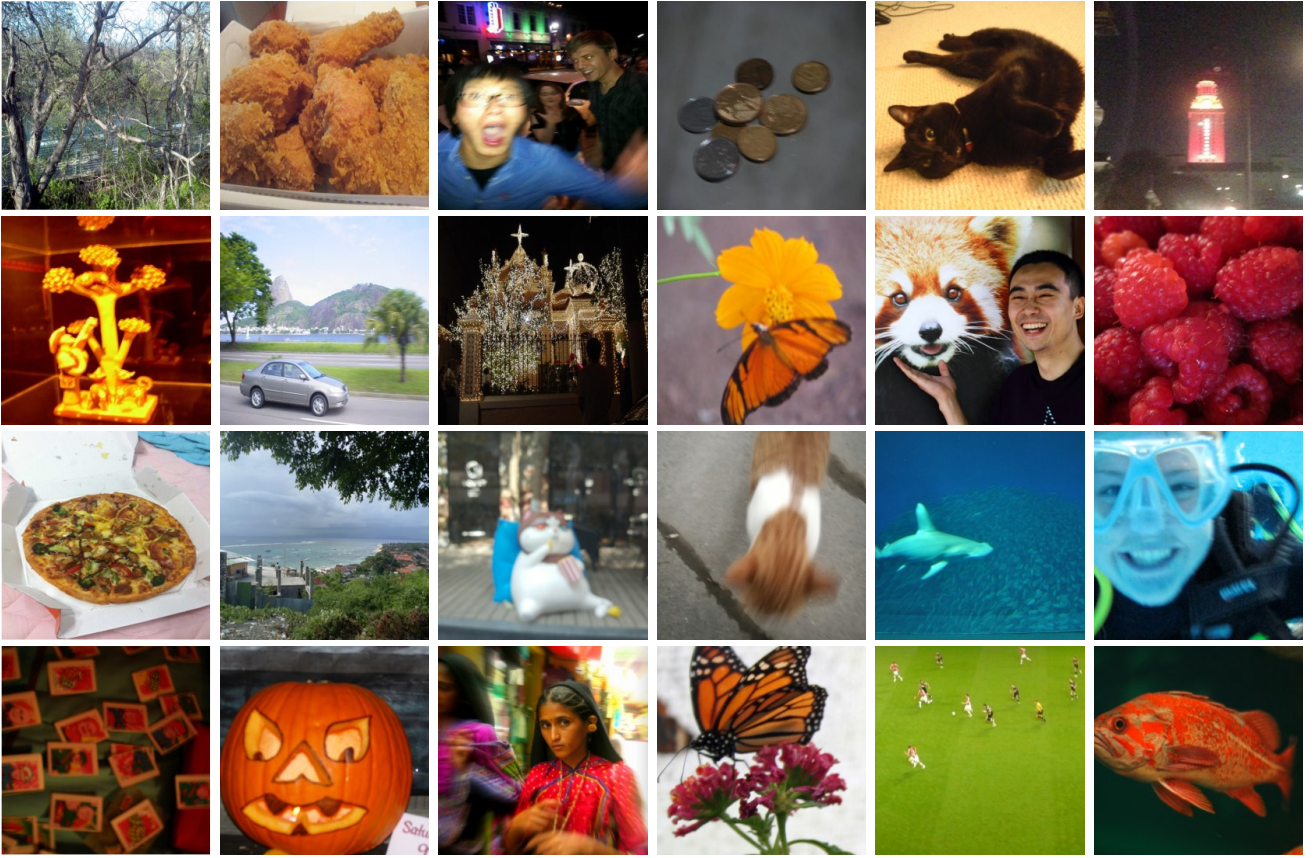


Fig. 4. Representative test photographic images to be enhanced.

LIQE 1.220	MUSIQ 1.088	UNIQUE 0.870	HyperIQA 0.433	DBCNN 0.294	CLIQQA+ -0.812	PaQ-2-PiQ -0.886	NIQE -2.218
---------------	----------------	-----------------	-------------------	----------------	-------------------	---------------------	----------------

Fig. 5. Global ranking scores of eight NR-IQA models using diffusion latent MAP estimation (higher scores indicate better performance). Models grouped within the same colored box have statistically indistinguishable performance, according to a two-tailed  $t$ -test.

learning to rank the perceived quality of image pairs sampled across multiple datasets.

- **MUSIQ** [19] is a multi-scale image quality Transformer [93] that processes images of varying sizes and aspect ratios to capture quality at different granularities with hash-based space and scale embeddings.
- **CLIQQA+** [46] extends a pretrained CLIP model [94] through prompt learning [95] for improved quality prediction accuracy on KonIQ-10k [17].
- **LIQE** [11] also relies on a pretrained CLIP model. Unlike CLIQQA+ [94], it uses a set of fixed textural templates but finetunes both textual and visual encoders on multiple IQA datasets, similar to UNIQUE [40]. Additionally, LIQE jointly tackles two auxiliary tasks—scene classification and distortion type identification—alongside the primary quality prediction task.

We summarize the detailed specifications of these NR-IQA models in Table I.

**Image Fidelity Measure.** The chosen image fidelity term  $D_0(\cdot, \cdot)$  shall preserve the visual content and appearance of the

initial image  $\mathbf{x}^{\text{init}}$  while allowing the introduction of plausible details for enhancement. To achieve this, we measure the Euclidean distance between the optimized image and the initial image at a reduced resolution:

$$D_0(\mathbf{x}, \mathbf{x}^{\text{init}}) = \|\mathbf{x}_{\downarrow s} - \mathbf{x}_{\downarrow s}^{\text{init}}\|_2, \quad (20)$$

where  $\downarrow_s$  represents spatial downsampling by a factor of  $s$  using bicubic interpolation.

**Optimization Details.** In line with the recommendations of the Video Quality Experts Group [96], we adopt a four-parameter logistic function to compensate for the prediction nonlinearity inherent in NR-IQA models:

$$q_{\xi} \circ q_w(\mathbf{x}) = \frac{\xi_1 - \xi_2}{1 + \exp\left(\frac{q_w(\mathbf{x}) - \xi_3}{|\xi_4|}\right)} + \xi_2, \quad (21)$$

where  $\circ$  indicates function composition. To constrain the mapping range, we manually set  $\xi_1 = 1$  and  $\xi_2 = 0$ , representing the maximum and minimum values, respectively.  $\xi_3$  and  $\xi_4$  are learnable parameters. By integrating  $q_{\xi}(\cdot)$  as part of the NR-IQA model, the selection of the trade-off parameter  $\lambda$  in diffusion latent MAP estimation is significantly simplified.

TABLE I

GLOBAL RANKING RESULTS OF EIGHT NR-IQA MODELS. SMALLER RANKS SIGNIFY BETTER PERFORMANCE. “MULTIPLE” IN THE SECOND COLUMN INDICATES THAT UNIQUE AND LIQE ARE TRAINED ON A COMBINED DATASET COMPRISING LIVE, CSIQ, BID, CLIVE, KONIQ-10K, AND KADID-10K. SRCC RESULTS ARE ALSO INCLUDED IN THE FOURTH COLUMN (IN BRACKETS)

NR-IQA Model	Training Set	# of Params (in Millions)	SRCC Rank	MAP Rank	$\Delta$ Rank
NIQE [25]	–	0.001	8 (0.706)	8	0
CLIQQA+ [46]	KonIQ-10k	101.349	2 (0.855)	6	-4
PaQ-2-PiQ [39]	FLIVE	11.704	5 (0.827)	7	-2
HyperIQA [92]	KonIQ-10k	27.375	7 (0.776)	4	3
MUSIQ [19]	KonIQ-10k	27.125	3 (0.853)	2	1
DBCNN [30]	KonIQ-10k	15.311	6 (0.789)	5	1
UNIQUE [40]	Multiple	22.322	4 (0.838)	3	1
LIQE [11]	Multiple	150.976	1 (0.881)	1	0

We plug Stable Diffusion 2.0 [97] into EDICT, which is augmented by a ControlNet [98] to explicitly condition the generation process on the input image [74]. The ControlNet has been trained on massive low- and high-quality image pairs [99], [100].

Following [13], we configure EDICT with a mixing parameter of  $p = 0.93^{50/T}$  (in Eqs. (10) and (11)) and set the number of diffusion steps to  $T = 20$ . We set  $\lambda = 0.01$  to balance the magnitudes of the fidelity and prior terms in Eq. (17). Each image is optimized for up to  $\text{MaxIter} = 40$  iterations, with a learning rate  $\alpha = 2$  and a momentum parameter  $\rho = 0.9$ . Last, we set  $\gamma = 0.1$  (in Eq. (18)) to select image pairs for debiased psychophysical testing.

**Psychophysical Testing Details.** The psychophysical experiment was carried out in an indoor office environment illuminated by normal lighting sources (approximately 200 lux), with non-reflective ceilings, walls, and floors. The peak luminance of the display was set to  $200 \text{ cd/m}^2$ . All image pairs were presented at the actual resolution on a calibrated true-color LCD monitor, arranged in randomized spatial order. The viewing distance was fixed at 32 pixels per degree of visual angle. The 2AFC method was employed, in which subjects were forced to select the image of higher perceived quality. A total of 25 human subjects with normal or corrected-to-normal vision (13 males and 12 females), aged 23 to 36, participated in the study. A training session was included to familiarize subjects with the testing procedure. To mitigate fatigue effects, subjects were allowed to take breaks as needed at any time.

### B. Model Comparison Results

**Quantitative Results.** After psychophysical testing, we obtain the global ranking scores of the eight NR-IQA models using Eq. (19). We accompany the ranking results with a two-tailed  $t$ -test [101]. The null hypothesis assumes that the global ranking scores  $\mu_i$  and  $\mu_j$ , corresponding to the  $i$ -th and  $j$ -th NR-IQA models, respectively, are drawn from the same Normal distribution. If the test fails to reject the null hypothesis at the 5% significance level, the performance of the two NR-IQA models is considered statistically indistinguishable.

From the results in Fig. 5, we draw several interesting observations. First, LIQE [11] and UNIQUE [40] statistically significantly outperform most other methods, with the exception of MUSIQ [19]. This highlights the effectiveness of ranking image quality across multiple datasets. The performance

gap between LIQE and UNIQUE can be attributed to two primary factors: (1) the choice of backbone networks and (2) the volume of pretraining data. LIQE leverages a CLIP model with over 150 million parameters, trained on 400 million image-text pairs, whereas UNIQUE uses a ResNet-34 variant with approximately 22 million parameters, trained on 1.28 million images from ImageNet [102]. Second, despite MUSIQ, DBCNN [30], and HyperIQA [92] having similar model capacity and being trained on the same dataset (see Table I), MUSIQ significantly outperforms HyperIQA and DBCNN due to its multi-scale image representation, closely aligning with human visual perception. Third, CLIPIQA+ [46] exhibits relatively poor performance, which may seem surprising given that it shares the CLIP backbone with the top-performing LIQE. A deeper investigation reveals that CLIPIQA+ relies on prompt learning [95], keeping the model weights fixed. This likely restricts CLIPIQA+ from effectively learning or eliciting quality-aware computations. Fourth, the knowledge-driven NIQE [25], while designed to handle arbitrary distortions, performs poorly under our diffusion latent MAP estimation framework. This underscores the inherent difficulty of (manually) crafting features to capture the complex interactions between image statistics and realistic distortions.

We further compare the ranking results of the proposed diffusion latent MAP estimation framework with those obtained using Spearman’s rank correlation coefficient (SRCC) on the SPAQ dataset [18]. Note that all NR-IQA models are evaluated in a cross-dataset setting, as they have not been trained on SPAQ. A key observation from Table I is that higher SRCC performance does not necessarily translate to diffusion latent MAP estimation. In summary, our framework excels in discriminating the relative performance of NR-IQA models through analysis by synthesis, offering a complementary perspective to correlation-based performance measures.

**Qualitative Results.** We show representative MAP-enhanced images associated with different pairs of NR-IQA models in Fig. 6, identified automatically using Eq. (18). We begin by comparing LIQE and MUSIQ, the top two NR-IQA models in diffusion latent MAP estimation. As shown in Fig. 6(e), LIQE effectively removes the blur near the tail of the animal, restoring natural fur textures. In contrast, the enhanced image by MUSIQ introduces noticeable hallucination artifacts, with overly magnified and unnatural fine hair at the tail boundary (see Fig. 6(i)). However, LIQE does not enhance stamps as

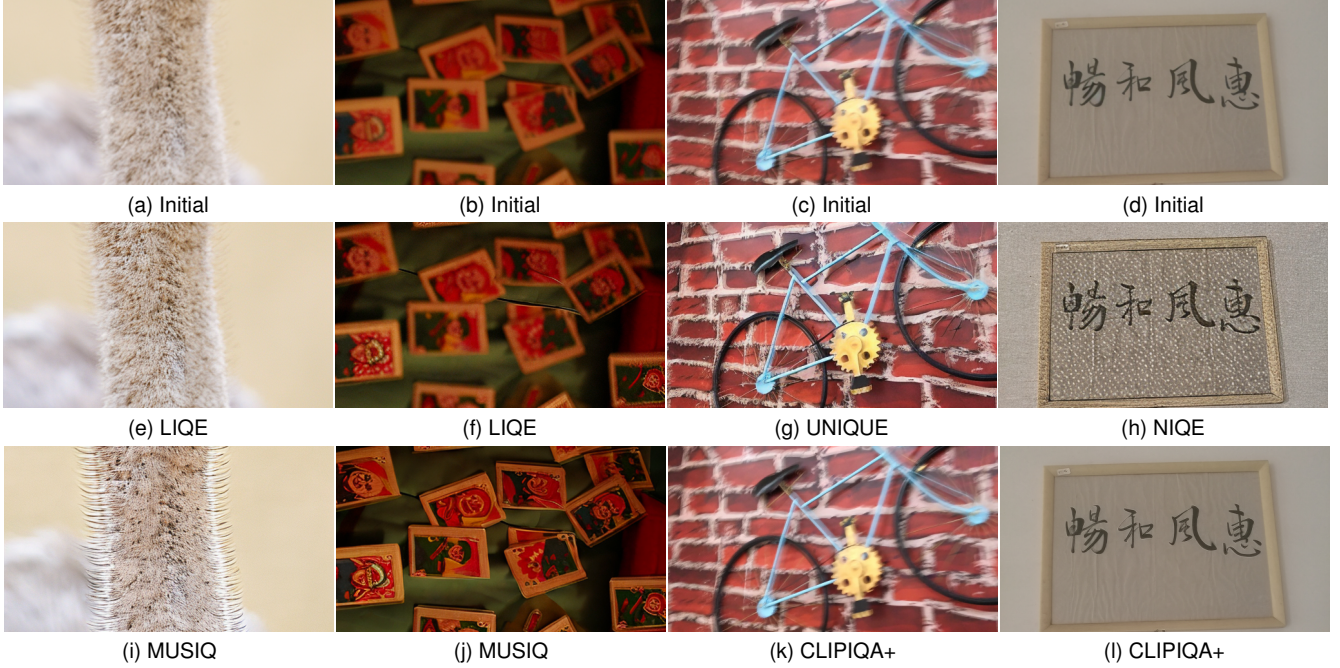


Fig. 6. Visual comparison of MAP-enhanced images associated with different pairs of NR-IQA models.

well as MUSIQ (see Figs. 6(f) and (j)), suggesting distinct strengths and weaknesses of each model. Turning our attention to CLIPIQA+, another CLIP-based NR-IQA model, we find that it induces a conservative approach, resulting in minimal perceptually meaningful pixel changes (see Figs. 6(k) and (l)). This restraint can be advantageous or disadvantageous depending on the input image quality. For high-quality inputs, such as Fig. 6(d), avoiding pixel modifications is wiser than introducing noticeable distortions, as done by NIQE in Fig. 6(h). Conversely, for low-quality inputs, more aggressive enhancement strategies, like those applied by UNIQUE in Fig. 6(g), tend to produce better results.

### C. Ablation Studies

To validate the chosen backbone diffusion model, we compare it against vanilla Stable Diffusion 2.0 operating without any ControlNet [98]. A detailed visual inspection of the MAP-enhanced images in Fig. 7 reveals a critical limitation of the vanilla model: its propensity to generate hallucinated, over-smooth, and cartoon-like content [103]. This issue is rooted in the inherent bias and randomness of diffusion models in image generation [104]. In contrast, the ControlNet-augmented variant leverages input images as conditioning, which introduces an implicit fidelity constraint that complements the explicit fidelity term in Eq. (17). This dual mechanism establishes a superior balance between image fidelity and visual quality.

We proceed to evaluate the image fidelity term by comparing our diffusion latent MAP estimation with direct diffusion latent optimization [12], *i.e.*,  $\arg \max_{\mathbf{x}_T} q_w(\mathbf{h}(\mathbf{x}_T))$ , which is equivalent to setting  $\lambda \rightarrow \infty$  in Eq. (17). As shown in Figs. 8(b) and (c), while both methods successfully improve the visual quality of the input image, our diffusion latent MAP estimation demonstrates better color fidelity to the

initial, making it particularly suitable for practical and robust enhancement of photographic images.

## V. NR-IQA MODEL IMPROVEMENT

Building on the model comparison results in Sec. IV-B, we advance further by designing a new NR-IQA model that integrates the strengths of the top-performing models. Specifically, we seek to: (1) adopt the CLIP backbone from LIQE, which benefits from a large model capacity with weights pretrained from web-scale data; (2) preserve the mixed-dataset training strategy employed by both LIQE and UNIQUE; and (3) incorporate the multi-scale image representation of MUSIQ.

### A. Improved Model Design

The original LIQE corresponds an input image  $\mathbf{x}$  to multiple textual templates, yielding a joint probability distribution over predictions across three tasks: NR-IQA, scene classification, and distortion type identification. In this work, we focus solely on the NR-IQA task, working with a Likert-scale of five quality levels:  $v \in \mathcal{V} = \{1, 2, 3, 4, 5\} = \{\text{“bad”}, \text{“poor”}, \text{“fair”}, \text{“good”}, \text{“perfect”}\}$  and relating discrete  $v$  to continuous quality estimate  $q_w(\mathbf{x})$  by

$$q_w(\mathbf{x}) = \sum_{v=1}^V p_w(v|\mathbf{x}) \times v, \quad (22)$$

where  $p_w(v|\mathbf{x})$  is the estimated probability of image  $\mathbf{x}$  at quality level  $v$  and  $V = 5$ . Built on the CLIP backbone [94], LIQE comprises an image encoder  $\mathbf{f}_\phi(\cdot) : \mathbb{R}^M \mapsto \mathbb{R}^L$  and a language encoder  $\mathbf{g}_\varphi(\cdot) : \mathcal{T} \mapsto \mathbb{R}^L$  that have the same output feature dimension, parameterized by  $\phi$  and  $\varphi$ , respectively, which constitute the parameter vector  $\mathbf{w}$ .  $\mathcal{T}$  represents the text corpus. The image encoder  $\mathbf{f}_\phi(\cdot)$  generates a visual





Fig. 7. Visual comparison of MAP-enhanced images using vanilla Stable Diffusion 2.0 and its ControlNet-augmented variant.

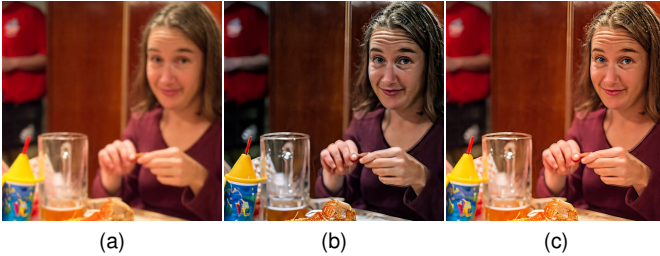


Fig. 8. (a) Initial image with mixed realistic degradations. (b) Enhanced image by direct diffusion latent optimization of LIQE [11] (corresponding to diffusion latent MAP estimation with  $\lambda = \infty$ ), with an overall color appearance that undesirably diverges from (a). (c) Enhanced image by the proposed diffusion latent MAP estimation with respect to LIQE [11].

embedding matrix  $\mathbf{F}(\mathbf{x}) \in \mathbb{R}^{U \times L}$  from  $U$  sub-images cropped from  $\mathbf{x}$ . Each sub-image has a fixed resolution of  $224 \times 224 \times 3$ , consistent with the CLIP model design. Unlike LIQE, which directly crops sub-images at the original image resolution, the improved model relies on a multi-scale image representation. Specifically, we construct a three-level image pyramid from  $\mathbf{x}$  using bicubic interpolation. The bottom level retains the original resolution, the middle level is resized by a factor of 0.75, and the top level is resized such that the shorter side has 224 pixels while keeping the aspect ratio. Sub-images of size  $224 \times 224 \times 3$  are then cropped from all three levels of the image pyramid. On the other hand, given  $V$  textual templates, the language encoder produces a textual embedding matrix  $\mathbf{G}(\mathbf{x}) \in \mathbb{R}^{V \times L}$ .

We follow LIQE to compute the cosine similarity between the visual embedding of the  $u$ -th sub-image  $\mathbf{F}_{u\bullet}$  and the  $v$ -th textual embedding  $\mathbf{G}_{v\bullet}$ , averaging across  $U$  sub-images to

obtain the image-level correspondence score:

$$\text{logit}_w(v|\mathbf{x}) = \frac{1}{U} \sum_{u=1}^U \frac{\mathbf{F}_{u\bullet}(\mathbf{x}) \mathbf{G}_{v\bullet}^T(\mathbf{x})}{\|\mathbf{F}_{u\bullet}(\mathbf{x})\|_2 \|\mathbf{G}_{v\bullet}(\mathbf{x})\|_2}. \quad (23)$$

We apply a softmax function to compute the probability distribution over all quality levels with a learned temperature parameter  $\tau$ :

$$p_w(v|\mathbf{x}) = \frac{\exp(\text{logit}_w(v|\mathbf{x})/\tau)}{\sum_v \exp(\text{logit}_w(v|\mathbf{x})/\tau)}. \quad (24)$$

After computing  $p_w(v|\mathbf{x})$ , we plug it into Eq. (22) to obtain the quality estimate  $q_w(\mathbf{x})$ . Similar to LIQE and UNIQUE, we employ pairwise learning-to-rank for model parameter estimation across multiple IQA datasets. Specifically, for an image pair  $(\mathbf{x}, \mathbf{y})$  from the same dataset, we assign a binary label according to their ground-truth MOSs  $q(\mathbf{x})$  and  $q(\mathbf{y})$ :

$$p(\mathbf{x}, \mathbf{y}) = \begin{cases} 1 & \text{if } q(\mathbf{x}) \geq q(\mathbf{y}) \\ 0 & \text{otherwise} \end{cases}. \quad (25)$$

Under the Thurstone model [88], the probability that  $\mathbf{x}$  is of higher quality than  $\mathbf{y}$  is estimated as:

$$p_w(\mathbf{x}, \mathbf{y}) = \Phi \left( \frac{q_w(\mathbf{x}) - q_w(\mathbf{y})}{\sqrt{2}} \right). \quad (26)$$

Same as in [11], [40], we adopt the fidelity function [105] as the loss:

$$\ell_w(\mathbf{x}, \mathbf{y}) = 1 - \sqrt{p(\mathbf{x}, \mathbf{y}) p_w(\mathbf{x}, \mathbf{y})} - \sqrt{(1 - p(\mathbf{x}, \mathbf{y}))(1 - p_w(\mathbf{x}, \mathbf{y}))}. \quad (27)$$

We term the resulting NR-IQA model as multi-scale LIQE (MS-LIQE). Training was carried out by AdamW [106] with a decoupled weight decay of  $10^{-3}$  and a mini-batch size

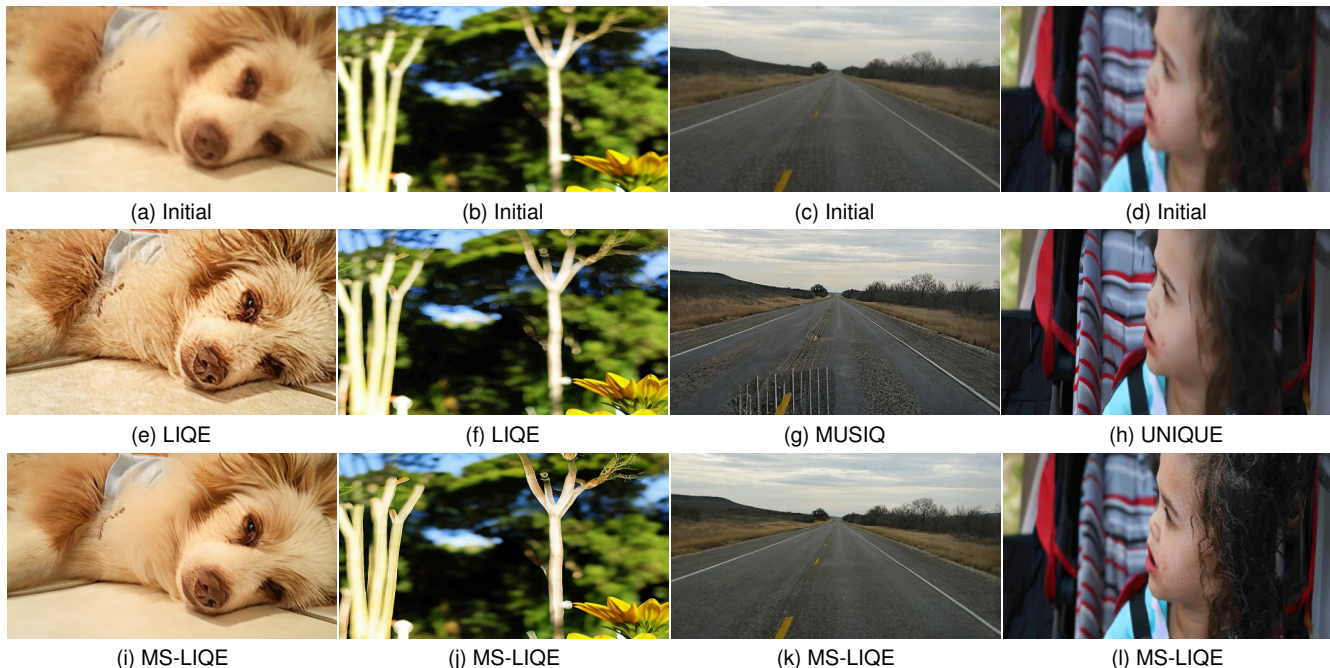


Fig. 9. Visual comparison of MAP-enhanced images produced by MS-LIQE and the three NR-IQA models as inspiration.

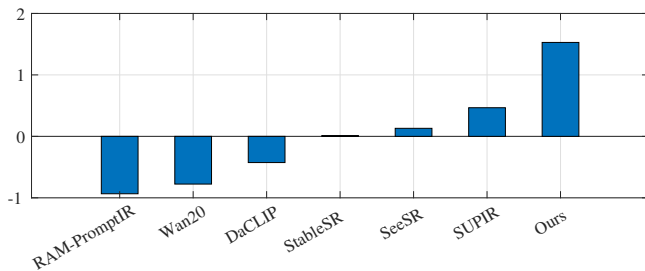


Fig. 10. Global ranking scores of real-world image enhancers.

of 48. The initial learning rate was set to  $5 \times 10^{-6}$ , which was scheduled by a cosine annealing rule [107]. We optimized MS-LIQE for 80 epochs on the combined LIVE [20], CSIQ [21], BID [22], LIVE Challenge [16], KonIQ-10k [17], and KADID-10k [23] datasets.

### B. Improved Model Results

We compare MS-LIQE against LIQE, MUSIQ, and UNIQUE (the three NR-IQA models that inspire the development of MS-LIQE) in the proposed diffusion latent MAP estimation framework. To quantitatively evaluate visual quality improvements, we again employ the debiased psychophysical testing (described in Sec. III-C) on the  $3 \times 20$  sampled image pairs. The results indicate a clear preference among subjects for the MAP-enhanced images by MS-LIQE, which garners 76.4%, 78.6%, and 82.5% of the votes compared to LIQE, MUSIQ, and UNIUEQ, respectively. In Fig. 9(i), MS-LIQE reduces noisy and grainy artifacts in the fur and background regions, and offers more natural textures and tones, compared to LIQE. In Fig. 9(j), MS-LIQE demonstrates superior handling of depth of focus, distinguishing three depth planes:

foreground flowers, midground stems, and background trees. In contrast, LIQE blends the midground and the background. These improvements can be attributed to the multi-scale image representation in MS-LIQE, which enhances its ability to perceive variations between objects at varying distances. Compared to MUSIQ, the image enhanced by MS-LIQE is clearer and more realistic. While there may be some contrast improvements by MUSIQ, the overall natural appearance is somewhat compromised, due to the introduction of noticeable artifacts, especially in the lower section of the road in Fig. 9(g). In comparison to UNIQUE, MS-LIQE produces the most refined and natural-looking result, with improved sharpness and clarity, especially in the hair textures. UNIQUE, however, focuses undesirably on removing the background out-of-focus blur.

### C. Comparison with Different Real-world Image Enhancers

It is important to test the potential of our diffusion latent MAP estimation framework (equipped with MS-LIQE) in real-world image enhancement by comparing it against recent image enhancers, particularly those designed to handle complex, real-world degradations. We identify three categories of competing enhancers in the literature. (1) **All-in-one/Universal Image Restoration**: These models aim to address multiple degradations within a single network [111]. We include the latest DaCLIP [110] and RAM [112]. DaCLIP incorporates a degradation-aware CLIP within a generative model [110], whereas RAM adopts a PromptIR [108] backbone and is trained discriminatively; (2) **Real-world Image Super-resolution**: These methods adapt the generative capabilities of diffusion models to both upscale image resolution and mitigate common degradations such as noise, blur, and compression artifacts. We include StableSR [71],

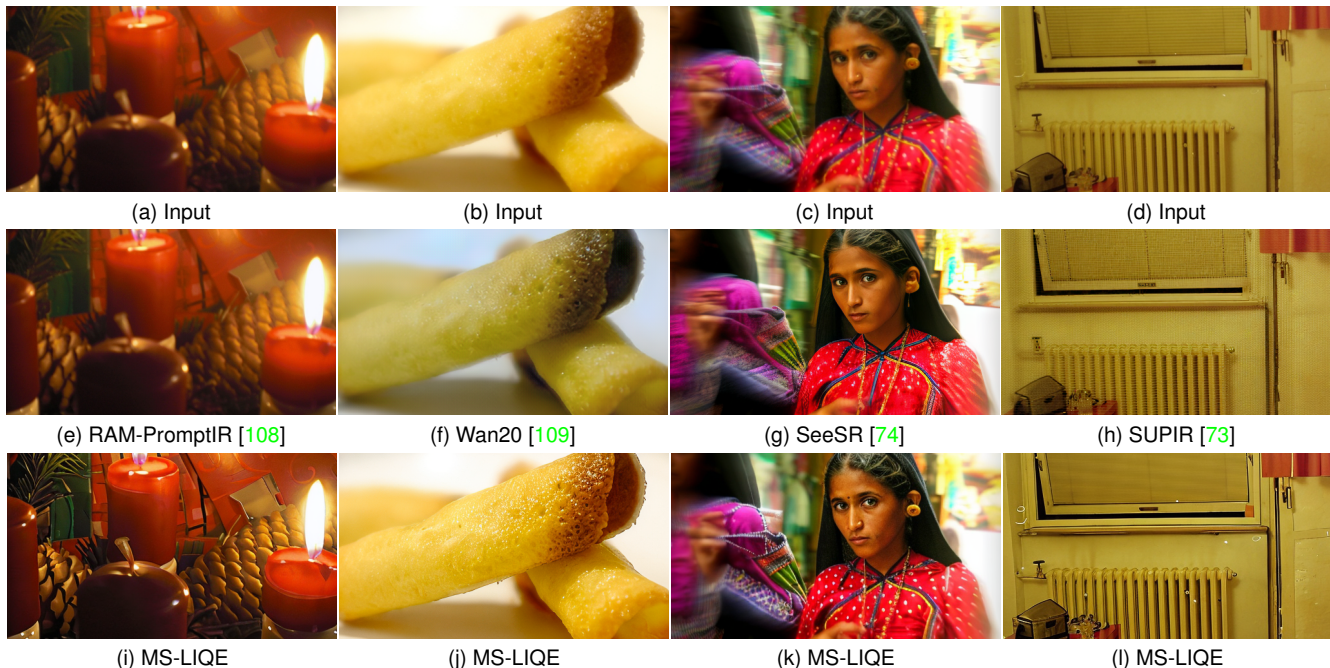


Fig. 11. Visual comparison of our MAP-enhanced images against results generated by other real-world image enhancers.

SeeSR [74], and SUPIR [73]. Here we evaluate their ability to enhance image quality at the original resolution; (3) **Old Photo Restoration**: These methods focus on restoring old and severely corrupted photographs. We include Wan20 [109], which trains a variational auto-encoder on triplets of real old photos, synthetic degraded images, and clean images.

To ensure a fair and quantitative comparison, we once again employ the debiased psychophysical testing on the  $\binom{7}{2} \times 20 = 420$  sampled image pairs, followed by global ranking aggregation using Eq. (19). From the results in Fig. 10, we have three major observations. First, our training-free diffusion latent MAP estimation method demonstrates a significant performance advantage over other enhancement techniques. Second, the relatively poor performance of the discriminative RAM-PromptIR highlights the inherent difficulty of directly mapping low-quality to high-quality images in the presence of real-world degradations. Third, incorporating generative priors markedly boosts the image enhancement performance, with stronger priors (e.g., SDXL [113] used in SUPIR) yielding even greater improvements.

We present representative visual examples in Fig. 11 to facilitate an intuitive comparison of the enhanced results. As shown in Fig. 11(e), RAM-PromptIR introduces minimal modifications to the input image. This behavior likely stems from the fact that the complex real-world degradations fall outside the training distribution of RAM-PromptIR, rendering it ineffective in identifying the degraded regions requiring enhancement. In contrast, our method preserves details in both the shadows and highlights satisfactorily. The resulting image has better contrast and a natural look, making it visually more appealing. Compared to Wan20, our enhanced result has more natural-looking details, vivid colors, and well-preserved textures. Importantly, it is more faithful to the input image,

highlighting the necessity of the fidelity term in Eq. (17). Large diffusion-based super-resolution methods tend to be aggressive, producing images that appear higher quality than the input at first sight. However, compared to the MAP-enhanced images, their results exhibit lower fidelity to the input, evidenced by undesired alterations in facial semantics (Fig. 11(g)) and reduced quality caused by the grainy artifacts (Fig. 11(h)). These results showcase the promise of diffusion latent MAP estimation in real-world image enhancement when working with a proper NR-IQA model (MS-LIQE in this case).

#### D. Post-enhancement Results

The proposed diffusion latent MAP estimation framework is orthogonal to current real-world image enhancers, and can serve as a post-enhancement step to further refine their outputs. To evaluate this, we show in Fig. 12 image triplets, consisting of the low-quality inputs, the outputs from base enhancers, and our MAP-refined results. It is evident that our method is helpful for all base enhancers across diverse natural scenes, enhancing the perceived quality of their outputs while ensuring content fidelity. Improvements are achieved through distortion removal (e.g., grainy artifacts in Fig. 12(e) and blur in Fig. 12(f)), texture enrichment (in Figs. 12(g) and (k)), and detail enhancement (in Figs. 12(h) and (l)).

## VI. CONCLUSION AND DISCUSSION

We have developed diffusion latent MAP estimation, a computational framework that, for the first time, enables existing “imperfect” NR-IQA models to tackle challenging real-world image enhancement. The core innovation lies in augmenting NR-IQA models with a differentiable and bijective diffusion transform. Given the diverse design principles and implementation details of NR-IQA models, they naturally yield

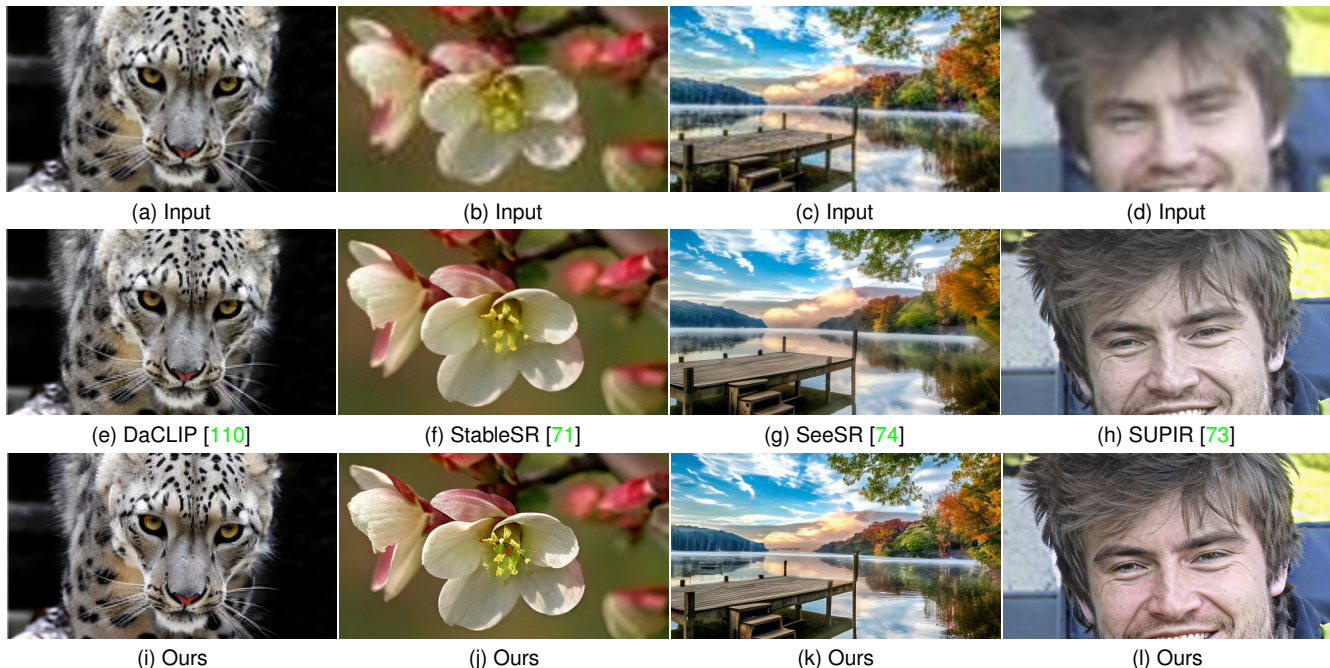


Fig. 12. Visual examples of MAP-refined images from outputs generated by different real-world image enhancers.

distinct enhancement results for the same input image. This variability allows for a comparative evaluation of NR-IQA models in terms of their image enhancement ability, aligning with the fundamental idea of analysis by synthesis. We have systematically compared eight NR-IQA models using diffusion latent MAP estimation, offering a complementary perspective to conventional correlation-based evaluations. Furthermore, we demonstrated the utility of diffusion latent MAP estimation in NR-IQA model improvement by combining the advantages of top-performing NR-IQA models in the framework. This fosters a constructive feedback loop between model evaluation and development. The resulting NR-IQA model demonstrated improved real-world image enhancement performance.

In the future, we aim to develop a general and robust MAP solution for real-world image enhancement. Currently, the success of our framework hinges on the ability of NR-IQA models to accurately evaluate image quality. A significant challenge lies in mitigating the phenomenon of shortcut learning [114], which may lead NR-IQA models to just output higher-quality predictions without inducing any perceptually meaningful enhancement [115]. To address this, a promising direction is to design generative NR-IQA models, which estimate the conditional probability of a test image given the quality score (*i.e.*,  $p(\mathbf{x}|q)$ ), rather than predicting the quality score from the image (*i.e.*,  $p(q|\mathbf{x})$ ), as done by most existing NR-IQA models. Additionally, reducing the computational complexity of gradient calculations across the entire (reverse) diffusion process presents another practical avenue for advancement [116]–[118].

## REFERENCES

- [1] Z. Wang and A. C. Bovik, *Modern Image Quality Assessment*. Morgan & Claypool, 2006.
- [2] Z. Wang, A. C. Bovik, H. R. Sheikh, and E. P. Simoncelli, “Image quality assessment: From error visibility to structural similarity,” *IEEE Transactions on Image Processing*, vol. 13, no. 4, pp. 600–612, Apr. 2004.
- [3] R. Zhang, P. Isola, A. A. Efros, E. Shechtman, and O. Wang, “The unreasonable effectiveness of deep features as a perceptual metric,” in *IEEE/CVF Conference on Computer Vision and Pattern Recognition*, 2018, pp. 586–595.
- [4] A. Mittal, A. K. Moorthy, and A. C. Bovik, “No-reference image quality assessment in the spatial domain,” *IEEE Transactions on Image Processing*, vol. 21, no. 12, pp. 4695–4708, Dec. 2012.
- [5] S. Bosse, D. Maniry, K. Müller, T. Wiegand, and W. Samek, “Deep neural networks for no-reference and full-reference image quality assessment,” *IEEE Transactions on Image Processing*, vol. 27, no. 1, pp. 206–219, Jan. 2018.
- [6] P. Cao, Z. Wang, and K. Ma, “Debiased subjective assessment of real-world image enhancement,” in *IEEE/CVF Conference on Computer Vision and Pattern Recognition*, 2021, pp. 711–721.
- [7] K. Ding, K. Ma, S. Wang, and E. P. Simoncelli, “Image quality assessment: Unifying structure and texture similarity,” *IEEE Transactions on Pattern Analysis and Machine Intelligence*, vol. 44, no. 5, pp. 2567–2581, May 2022.
- [8] —, “Comparison of full-reference image quality models for optimization of image processing systems,” *International Journal of Computer Vision*, vol. 129, no. 4, pp. 1258–1281, Apr. 2021.
- [9] U. Grenander and M. I. Miller, *Pattern Theory: From Representation to Inference*. Oxford University Press, 2007.
- [10] W. Zhang, D. Li, X. Min, G. Zhai, G. Guo, X. Yang, and K. Ma, “Perceptual attacks of no-reference image quality models with human-in-the-loop,” in *Advances in Neural Information Processing Systems*, 2022, pp. 2916–2929.
- [11] W. Zhang, G. Zhai, Y. Wei, X. Yang, and K. Ma, “Blind image quality assessment via vision-language correspondence: A multitask learning perspective,” in *IEEE/CVF Conference on Computer Vision and Pattern Recognition*, 2023, pp. 14 071–14 081.
- [12] B. Wallace, A. Gokul, S. Ermon, and N. Naik, “End-to-end diffusion latent optimization improves classifier guidance,” in *IEEE/CVF International Conference on Computer Vision*, 2023, pp. 7280–7290.
- [13] B. Wallace, A. Gokul, and N. Naik, “EDICT: Exact diffusion inversion via coupled transformations,” in *IEEE/CVF Conference on Computer Vision and Pattern Recognition*, 2023, pp. 22 532–22 541.
- [14] L. Dinh, D. Krueger, and Y. Bengio, “NICE: Non-linear independent components estimation,” in *International Conference on Learning Representations Workshops*, 2015.

- [15] L. Dinh, J. Sohl-Dickstein, and S. Bengio, "Density estimation using real NVP," in *International Conference on Learning Representations*, 2017.
- [16] D. Ghadiyaram and A. C. Bovik, "Massive online crowdsourced study of subjective and objective picture quality," *IEEE Transactions on Image Processing*, vol. 25, no. 1, pp. 372–387, Jan. 2016.
- [17] V. Hosu, H. Lin, T. Sziranyi, and D. Saupe, "KonIQ-10k: An ecologically valid database for deep learning of blind image quality assessment," *IEEE Transactions on Image Processing*, vol. 29, pp. 4041–4056, Jan. 2020.
- [18] Y. Fang, H. Zhu, Y. Zeng, K. Ma, and Z. Wang, "Perceptual quality assessment of smartphone photography," in *IEEE/CVF Conference on Computer Vision and Pattern Recognition*, 2020, pp. 3677–3686.
- [19] J. Ke, Q. Wang, Y. Wang, P. Milanfar, and F. Yang, "MUSIQ: Multi-scale image quality transformer," in *IEEE/CVF International Conference on Computer Vision*, 2021, pp. 5148–5157.
- [20] H. R. Sheikh, M. F. Sabir, and A. C. Bovik, "A statistical evaluation of recent full reference image quality assessment algorithms," *IEEE Transactions on Image Processing*, vol. 15, no. 11, pp. 3440–3451, Nov. 2006.
- [21] E. C. Larson and D. M. Chandler, "Most apparent distortion: Full-reference image quality assessment and the role of strategy," *Journal of Electronic Imaging*, vol. 19, no. 1, pp. 1–21, Jan. 2010.
- [22] A. Ciancio, A. L. N. T. Targino da Costa, E. A. B. da Silva, A. Said, R. Samadani, and P. Obrador, "No-reference blur assessment of digital pictures based on multifeature classifiers," *IEEE Transactions on Image Processing*, vol. 20, no. 1, pp. 64–75, Jan. 2011.
- [23] H. Lin, V. Hosu, and D. Saupe, "KADID-10k: A large-scale artificially distorted IQA database," in *IEEE International Conference on Multimedia and Expo*, 2019, pp. 1–3.
- [24] D. Mumford, "Pattern theory: A unifying perspective," in *European Congress of Mathematics*, 1994, pp. 187–224.
- [25] A. Mittal, R. Soundararajan, and A. C. Bovik, "Making a 'completely blind' image quality analyzer," *IEEE Signal Processing Letters*, vol. 20, no. 3, pp. 209–212, Mar. 2013.
- [26] A. K. Moorthy and A. C. Bovik, "Blind image quality assessment: From natural scene statistics to perceptual quality," *IEEE Transactions on Image Processing*, vol. 20, no. 12, pp. 3350–3364, Dec. 2011.
- [27] D. Ghadiyaram and A. C. Bovik, "Perceptual quality prediction on authentically distorted images using a bag of features approach," *Journal of Vision*, vol. 17, no. 1, pp. 32–32, Jan. 2017.
- [28] K. Ma, W. Liu, K. Zhang, Z. Duanmu, Z. Wang, and W. Zuo, "End-to-end blind image quality assessment using deep neural networks," *IEEE Transactions on Image Processing*, vol. 27, no. 3, pp. 1202–1213, Mar. 2018.
- [29] X. Liu, J. van de Weijer, and A. D. Bagdanov, "RankIQA: Learning from rankings for no-reference image quality assessment," in *IEEE/CVF International Conference on Computer Vision*, 2017, pp. 1040–1049.
- [30] W. Zhang, K. Ma, J. Yan, D. Deng, and Z. Wang, "Blind image quality assessment using a deep bilinear convolutional neural network," *IEEE Transactions on Circuit Systems and Video Technology*, vol. 30, no. 1, pp. 36–47, Jan. 2020.
- [31] K. Ma, X. Liu, Y. Fang, and E. P. Simoncelli, "Blind image quality assessment by learning from multiple annotators," in *IEEE International Conference on Image Processing*, 2019, pp. 2344–2348.
- [32] J. Wu, J. Ma, F. Liang, W. Dong, G. Shi, and W. Lin, "End-to-end blind image quality prediction with cascaded deep neural network," *IEEE Transactions on Image Processing*, vol. 29, pp. 7414–7426, Jun. 2020.
- [33] H. Zhu, L. Li, J. Wu, W. Dong, and G. Shi, "MetaIQA: Deep meta-learning for no-reference image quality assessment," in *IEEE/CVF Conference on Computer Vision and Pattern Recognition*, 2020, pp. 14 131–14 140.
- [34] P. C. Madhusudana, N. Birkbeck, Y. Wang, B. Adsumilli, and A. C. Bovik, "Image quality assessment using contrastive learning," *IEEE Transactions on Image Processing*, vol. 31, pp. 4149–4161, Jun. 2022.
- [35] K. Zhao, K. Yuan, M. Sun, M. Li, and X. Wen, "Quality-aware pre-trained models for blind image quality assessment," in *IEEE/CVF Conference on Computer Vision and Pattern Recognition*, 2023, pp. 22 302–22 313.
- [36] A. Saha, S. Mishra, and A. C. Bovik, "Re-IQA: Unsupervised learning for image quality assessment in the wild," in *IEEE/CVF Conference on Computer Vision and Pattern Recognition*, 2023, pp. 5846–5855.
- [37] L. Agnolucci, L. Galteri, M. Bertini, and A. Del Bimbo, "ARNIQA: Learning distortion manifold for image quality assessment," in *IEEE Winter Conference on Applications of Computer Vision*, 2024, pp. 189–198.
- [38] S. Su, V. Hosu, H. Lin, Y. Zhang, and D. Saupe, "KonIQ++: Boosting no-reference image quality assessment in the wild by jointly predicting image quality and defects," in *British Machine Vision Conference*, 2021, pp. 1–12.
- [39] Z. Ying, H. Niu, P. Gupta, D. Mahajan, D. Ghadiyaram, and A. C. Bovik, "From patches to pictures (PaQ-2-PiQ): Mapping the perceptual space of picture quality," in *IEEE/CVF Conference on Computer Vision and Pattern Recognition*, 2020, pp. 3572–3582.
- [40] W. Zhang, K. Ma, G. Zhai, and X. Yang, "Uncertainty-aware blind image quality assessment in the laboratory and wild," *IEEE Transactions on Image Processing*, vol. 30, pp. 3474–3486, Mar. 2021.
- [41] W. Zhang, D. Li, C. Ma, G. Zhai, X. Yang, and K. Ma, "Continual learning for blind image quality assessment," *IEEE Transactions on Pattern Analysis and Machine Intelligence*, vol. 45, no. 3, pp. 2864–2878, Mar. 2023.
- [42] W. Zhang, K. Ma, G. Zhai, and X. Yang, "Task-specific normalization for continual learning of blind image quality models," *IEEE Transactions on Image Processing*, vol. 33, pp. 1898–1910, 2024.
- [43] A. Li, J. Wu, Y. Liu, and L. Li, "Bridging the synthetic-to-authentic gap: Distortion-guided unsupervised domain adaptation for blind image quality assessment," in *IEEE/CVF Conference on Computer Vision and Pattern Recognition*, 2024, pp. 28 422–28 431.
- [44] S. Yang, T. Wu, S. Shi, S. Lao, Y. Gong, M. Cao, J. Wang, and Y. Yang, "MANIQA: Multi-dimension attention network for no-reference image quality assessment," in *IEEE/CVF Conference on Computer Vision and Pattern Recognition Workshops*, 2022, pp. 1191–1200.
- [45] C. Chen, J. Mo, J. Hou, H. Wu, L. Liao, W. Sun, Q. Yan, and W. Lin, "TOPIQ: A top-down approach from semantics to distortions for image quality assessment," *IEEE Transactions on Image Processing*, vol. 33, pp. 2404–2418, Mar. 2024.
- [46] J. Wang, K. C. Chan, and C. C. Loy, "Exploring CLIP for assessing the look and feel of images," in *AAAI Conference on Artificial Intelligence*, 2023, pp. 2555–2563.
- [47] H. Wu, Z. Zhang, W. Zhang, C. Chen, L. Liao, C. Li, Y. Gao, A. Wang, E. Zhang, W. Sun, Q. Yan, X. Min, G. Zhai, and W. Lin, "Q-Align: Teaching LMMs for visual scoring via discrete text-defined levels," in *International Conference on Machine Learning*, 2024, pp. 54 015–54 029.
- [48] H. Wu, Z. Zhang, E. Zhang, C. Chen, L. Liao, A. Wang, K. Xu, C. Li, J. Hou, G. Zhai, G. Xue, W. Sun, Q. Yan, and W. Lin, "Q-Instruct: Improving low-level visual abilities for multi-modality foundation models," in *IEEE/CVF Conference on Computer Vision and Pattern Recognition*, 2024, pp. 25 490–25 500.
- [49] T. Wu, K. Ma, J. Liang, Y. Yang, and L. Zhang, "A comprehensive study of multimodal large language models for image quality assessment," in *European Conference on Computer Vision*, 2024, pp. 143–160.
- [50] K. P. Burnham and D. R. Anderson, *Model Selection and Multi-model Inference: A Practical Information-Theoretic Approach*. Springer New York, 2004.
- [51] Z. Wang and E. P. Simoncelli, "Maximum differentiation (MAD) competition: A methodology for comparing computational models of perceptual quantities," *Journal of Vision*, vol. 8, no. 12, pp. 1–13, Sep. 2008.
- [52] A. Bernardino, J. Ballé, V. Laparra, and E. P. Simoncelli, "Eigen-distortions of hierarchical representations," in *Advances in Neural Information Processing Systems*, 2017, pp. 3531–3540.
- [53] T. Golan, P. C. Raju, and N. Kriegeskorte, "Controversial stimuli: Pitting neural networks against each other as models of human cognition," *Proceedings of the National Academy of Sciences*, vol. 117, no. 47, pp. 29 330–29 337, Nov. 2020.
- [54] K. Ma, Z. Duanmu, Z. Wang, Q. Wu, W. Liu, H. Yong, H. Li, and L. Zhang, "Group maximum differentiation competition: Model comparison with few samples," *IEEE Transactions on Pattern Analysis and Machine Intelligence*, vol. 42, no. 4, pp. 851–864, Apr. 2020.
- [55] H. Wang, T. Chen, Z. Wang, and K. Ma, "I am going MAD: Maximum discrepancy competition for comparing classifiers adaptively," in *International Conference on Learning Representations*, 2020.
- [56] J. Yan, Y. Zhong, Y. Fang, Z. Wang, and K. Ma, "Exposing semantic segmentation failures via maximum discrepancy competition," *International Journal of Computer Vision*, vol. 129, no. 5, pp. 1768–1786, Mar. 2021.
- [57] K. Feng, K. Ding, K. Ma, Z. Wang, Q. Zhang, and H. Chen, "Sample-efficient human evaluation of large language models via maximum discrepancy competition," *arXiv preprint arXiv:2404.08008*, 2024.

- [58] F.-A. Croitoru, V. Hondru, R. T. Ionescu, and M. Shah, "Diffusion models in vision: A survey," *IEEE Transactions on Pattern Analysis and Machine Intelligence*, vol. 45, no. 9, pp. 10 850–10 869, Sep. 2023.
- [59] J. Sohl-Dickstein, E. Weiss, N. Maheswaranathan, and S. Ganguli, "Deep unsupervised learning using nonequilibrium thermodynamics," in *International Conference on Machine Learning*, 2015, pp. 2256–2265.
- [60] J. Ho, A. Jain, and P. Abbeel, "Denoising diffusion probabilistic models," in *Advances in Neural Information Processing Systems*, 2020, pp. 6840–6851.
- [61] V. N. Pokrovskii, *Thermodynamics of Complex Systems: Principles and Applications*. IOP Publishing, 2020.
- [62] Y. Song and S. Ermon, "Generative modeling by estimating gradients of the data distribution," in *Advances in Neural Information Processing Systems*, 2019, pp. 11 918–11 930.
- [63] A. Hyvärinen and P. Dayan, "Estimation of non-normalized statistical models by score matching," *Journal of Machine Learning Research*, vol. 6, no. 4, pp. 695–709, 2005.
- [64] Y. Song, J. Sohl-Dickstein, D. P. Kingma, A. Kumar, S. Ermon, and B. Poole, "Score-based generative modeling through stochastic differential equations," in *International Conference on Learning Representations*, 2021.
- [65] P. Dhariwal and A. Nichol, "Diffusion models beat GANs on image synthesis," in *Advances in Neural Information Processing Systems*, 2021, pp. 8780–8794.
- [66] A. Q. Nichol and P. Dhariwal, "Improved denoising diffusion probabilistic models," in *International Conference on Machine Learning*, 2021, pp. 8162–8171.
- [67] C. Meng, Y. He, Y. Song, J. Song, J. Wu, J.-Y. Zhu, and S. Ermon, "SDEdit: Guided image synthesis and editing with stochastic differential equations," in *International Conference on Learning Representations*, 2021.
- [68] J. Ho and T. Salimans, "Classifier-free diffusion guidance," in *Advances in Neural Information Processing Systems Workshops*, 2021.
- [69] A. Hertz, R. Mokady, J. Tenenbaum, K. Aberman, Y. Pritch, and D. Cohen-Or, "Prompt-to-prompt image editing with cross-attention control," in *International Conference on Learning Representations*, 2023.
- [70] J. Song, C. Meng, and S. Ermon, "Denoising diffusion implicit models," in *International Conference on Learning Representations*, 2021.
- [71] J. Wang, Z. Yue, S. Zhou, K. C. Chan, and C. C. Loy, "Exploiting diffusion prior for real-world image super-resolution," *International Journal of Computer Vision*, pp. 5929—5949, 2024.
- [72] X. Lin, J. He, Z. Chen, Z. Lyu, B. Dai, F. Yu, Y. Qiao, W. Ouyang, and C. Dong, "DiffBIR: Towards blind image restoration with generative diffusion prior," in *European Conference on Computer Vision*, 2025, pp. 430–448.
- [73] F. Yu, J. Gu, Z. Li, J. Hu, X. Kong, X. Wang, J. He, Y. Qiao, and C. Dong, "Scaling up to excellence: Practicing model scaling for photo-realistic image restoration in the wild," in *IEEE/CVF Conference on Computer Vision and Pattern Recognition*, 2024, pp. 25 669–25 680.
- [74] R. Wu, T. Yang, L. Sun, Z. Zhang, S. Li, and L. Zhang, "SeeSR: Towards semantics-aware real-world image super-resolution," in *IEEE/CVF Conference on Computer Vision and Pattern Recognition*, 2024, pp. 25 456–25 467.
- [75] B. Kawar, M. Elad, S. Ermon, and J. Song, "Denoising diffusion restoration models," in *Advances in Neural Information Processing Systems*, 2022, pp. 23 593–23 606.
- [76] Y. Wang, J. Yu, and J. Zhang, "Zero-shot image restoration using denoising diffusion null-space model," in *International Conference on Learning Representations*, 2023.
- [77] H. Chung, J. Kim, M. T. McCann, M. L. Klasky, and J. C. Ye, "Diffusion posterior sampling for general noisy inverse problems," in *International Conference on Learning Representations*, 2023.
- [78] Y. Zhu, K. Zhang, J. Liang, J. Cao, B. Wen, R. Timofte, and L. Van Gool, "Denoising diffusion models for plug-and-play image restoration," in *IEEE/CVF Conference on Computer Vision and Pattern Recognition*, 2023, pp. 1219–1229.
- [79] L. Yang, Z. Zhang, Y. Song, S. Hong, R. Xu, Y. Zhao, W. Zhang, B. Cui, and M.-H. Yang, "Diffusion models: A comprehensive survey of methods and applications," *ACM Computing Surveys*, vol. 56, no. 4, pp. 1–39, Sep. 2023.
- [80] D. Geman and C. Yang, "Nonlinear image recovery with half-quadratic regularization," *IEEE Transactions on Image Processing*, vol. 4, no. 7, pp. 932–946, Jul. 1995.
- [81] L. I. Rudin, S. Osher, and E. Fatemi, "Nonlinear total variation based noise removal algorithms," *Physica D: Nonlinear Phenomena*, vol. 60, no. 1–4, pp. 259–268, Nov. 1992.
- [82] J. Portilla, V. Strela, M. J. Wainwright, and E. P. Simoncelli, "Image denoising using scale mixtures of Gaussians in the wavelet domain," *IEEE Transactions on Image Processing*, vol. 12, no. 11, pp. 1338–1351, Nov. 2003.
- [83] A. Buades, B. Coll, and J.-M. Morel, "A non-local algorithm for image denoising," in *IEEE/CVF Conference on Computer Vision and Pattern Recognition*, 2005, pp. 60–65.
- [84] J. Wright, Y. Ma, J. Mairal, G. Sapiro, T. S. Huang, and S. Yan, "Sparse representation for computer vision and pattern recognition," *Proceedings of the IEEE*, vol. 98, no. 6, pp. 1031–1044, Jun. 2010.
- [85] J.-F. Cai, E. J. Candès, and Z. Shen, "A singular value thresholding algorithm for matrix completion," *SIAM Journal on Optimization*, vol. 20, no. 4, pp. 1956–1982, Jan. 2010.
- [86] D. Ulyanov, A. Vedaldi, and V. Lempitsky, "Deep image prior," *International Journal of Computer Vision*, vol. 128, no. 7, pp. 1867–1888, Jul. 2020.
- [87] I. Goodfellow, J. Pouget-Abadie, M. Mirza, B. Xu, D. Warde-Farley, S. Ozair, A. Courville, and Y. Bengio, "Generative adversarial nets," in *Advances in Neural Information Processing Systems*, 2014, pp. 2672–2680.
- [88] L. L. Thurstone, "A law of comparative judgment," *Psychological Review*, vol. 34, pp. 273–286, Jul. 1927.
- [89] M. Perez-Ortiz and R. K. Mantiuk, "A practical guide and software for analysing pairwise comparison experiments," *arXiv preprint arXiv:1712.03686*, 2017.
- [90] M. Perez-Ortiz, A. Mikhailiuk, E. Zerman, V. Hulusic, G. Valenzise, and R. K. Mantiuk, "From pairwise comparisons and rating to a unified quality scale," *IEEE Transactions on Image Processing*, vol. 29, pp. 1139–1151, 2020.
- [91] K. Simonyan and A. Zisserman, "Very deep convolutional networks for large-scale image recognition," in *International Conference on Learning Representations*, 2015.
- [92] S. Su, Q. Yan, Y. Zhu, C. Zhang, X. Ge, J. Sun, and Y. Zhang, "Blindly assess image quality in the wild guided by a self-adaptive hyper network," in *IEEE/CVF Conference on Computer Vision and Pattern Recognition*, 2020, pp. 3667–3676.
- [93] A. Dosovitskiy, L. Beyer, K. Alexander, D. Weissenborn, X. Zhai, T. Unterthiner, M. Dehghani, M. Minderer, G. Heigold, S. Gelly, J. Uszkoreit, and N. Houlsby, "An image is worth 16×16 words: Transformers for image recognition at scale," in *International Conference on Learning Representations*, 2021.
- [94] A. Radford, J. W. Kim, C. Hallacy, A. Ramesh, G. Goh, S. Agarwal, G. Sastry, A. Askell, P. Mishkin, J. Clark, G. Krueger, and I. Sutskever, "Learning transferable visual models from natural language supervision," in *International Conference on Machine Learning*, 2021, pp. 8748–8763.
- [95] K. Zhou, J. Yang, C. C. Loy, and Z. Liu, "Learning to prompt for vision-language models," *International Journal of Computer Vision*, vol. 130, no. 9, pp. 2337–2348, Jul. 2022.
- [96] VQEG, "Final report from the Video Quality Experts Group on the validation of objective models of video quality assessment," 2003. [Online]. Available: <http://www.vqeg.org>
- [97] R. Rombach, A. Blattmann, D. Lorenz, P. Esser, and B. Ommer, "High-resolution image synthesis with latent diffusion models," in *IEEE/CVF Conference on Computer Vision and Pattern Recognition*, 2022, pp. 10 684–10 695.
- [98] L. Zhang, A. Rao, and M. Agrawala, "Adding conditional control to text-to-image diffusion models," in *IEEE/CVF International Conference on Computer Vision*, 2023, pp. 3836–3847.
- [99] T. Karras, S. Laine, and T. Aila, "A style-based generator architecture for generative adversarial networks," in *IEEE/CVF Conference on Computer Vision and Pattern Recognition*, 2019, pp. 4401–4410.
- [100] Y. Li, K. Zhang, J. Liang, J. Cao, C. Liu, R. Gong, Y. Zhang, H. Tang, Y. Liu, D. Demandolx, R. Ranjan, R. Timofte, and L. Van Gool, "LSDIR: A large scale dataset for image restoration," in *IEEE/CVF Conference on Computer Vision and Pattern Recognition*, 2023, pp. 1775–1787.
- [101] H. A. David, *The Method of Paired Comparisons*. Hafner Publishing Company, 1963.
- [102] J. Deng, W. Dong, R. Socher, L.-J. Li, K. Li, and L. Fei-Fei, "ImageNet: A large-scale hierarchical image database," in *IEEE/CVF Conference on Computer Vision and Pattern Recognition*, 2009, pp. 248–255.

- [103] S. K. Aithal, P. Maini, Z. C. Lipton, and J. Z. Kolter, “Understanding hallucinations in diffusion models through mode interpolation,” *arXiv preprint arXiv:2406.09358*, 2024.
- [104] Z. Kadkhodaie and E. P. Simoncelli, “Stochastic solutions for linear inverse problems using the prior implicit in a denoiser,” in *Advances in Neural Information Processing Systems*, 2021, pp. 13 242–13 254.
- [105] M.-F. Tsai, T.-Y. Liu, T. Qin, H.-H. Chen, and W.-Y. Ma, “FRank: A ranking method with fidelity loss,” in *ACM SIGIR Conference on Research and Development in Information Retrieval*, 2007, pp. 383–390.
- [106] I. Loshchilov and F. Hutter, “Decoupled weight decay regularization,” in *International Conference on Learning Representations*, 2019.
- [107] —, “SGDR: Stochastic gradient descent with warm restarts,” in *International Conference on Learning Representations*, 2017.
- [108] V. Potlapalli, S. W. Zamir, S. H. Khan, and F. Shahbaz Khan, “PromptIR: Prompting for all-in-one image restoration,” in *Advances in Neural Information Processing Systems*, 2023.
- [109] Z. Wan, B. Zhang, D. Chen, P. Zhang, D. Chen, J. Liao, and F. Wen, “Bringing old photos back to life,” in *IEEE/CVF Conference on Computer Vision and Pattern Recognition*, 2020, pp. 2747–2757.
- [110] Z. Luo, F. K. Gustafsson, Z. Zhao, J. Sjölund, and T. B. Schön, “Controlling vision-language models for universal image restoration,” in *International Conference on Learning Representations*, 2024.
- [111] B. Li, X. Liu, P. Hu, Z. Wu, J. Lv, and X. Peng, “All-in-one image restoration for unknown corruption,” in *IEEE/CVF Conference on Computer Vision and Pattern Recognition*, 2022, pp. 17 452–17 462.
- [112] C.-J. Qin, R.-Q. Wu, Z. Liu, X. Lin, C.-L. Guo, H. H. Park, and C. Li, “Restore anything with masks: Leveraging mask image modeling for blind all-in-one image restoration,” in *European Conference on Computer Vision*, 2024, pp. 364–380.
- [113] D. Podell, Z. English, K. Lacey, A. Blattmann, T. Dockhorn, J. Müller, J. Penna, and R. Rombach, “SDXL: Improving latent diffusion models for high-resolution image synthesis,” *arXiv preprint arXiv:2307.01952*, 2023.
- [114] R. Geirhos, J.-H. Jacobsen, C. Michaelis, R. Zemel, W. Brendel, M. Bethge, and F. A. Wichmann, “Shortcut learning in deep neural networks,” *Nature Machine Intelligence*, vol. 2, no. 11, pp. 665–673, Nov. 2020.
- [115] L. Weng, “Reward hacking in reinforcement learning.” 2024. [Online]. Available: <https://lilianweng.github.io/posts/2024-11-28-reward-hacking/>
- [116] G. Zhang, J. P. Lewis, and W. B. Kleijn, “Exact diffusion inversion via bidirectional integration approximation,” in *European Conference on Computer Vision*, 2024, pp. 19–36.
- [117] F. Wang, H. Yin, Y. Dong, H. Zhu, C. Zhang, H. Zhao, H. Qian, and C. Li, “BELM: Bidirectional explicit linear multi-step sampler for exact inversion in diffusion models,” in *Advances in Neural Information Processing Systems*, 2024.
- [118] Y. Song, P. Dhariwal, M. Chen, and I. Sutskever, “Consistency models,” in *International Conference on Machine Learning*, 2023, pp. 32 211–32 252.